Nonlinear actuation of smart composites using a coupled piezoelectric-mechanical model

INSTITUTE OF PHYSICS PUBLISHING SMART MATERIALS AND STRUCTURES
Smart Mater. Struct. **10** (2001) 743–749 PII: S0964-1726(01)24412-7

Nonlinear actuation of smart composites using a coupled piezoelectric–mechanical model

Robert P Thornburgh and Aditi Chattopadhyay

Department of Mechanical and Aerospace Engineering, Arizona State University, Tempe, AZ 85287-6106, USA

Received 17 January 2001, in final form 19 March 2001
Published 18 July 2001
Online at stacks.iop.org/SMS/10/743

Abstract
A completely coupled piezoelectric–mechanical theory which includes nonlinear piezoelectric effects has been developed for composite plates with embedded or surface bonded actuators and sensors. A higher-order laminate theory is used to describe the displacement field in order to accurately capture the effects of transverse shear in moderately thick laminates. The coupling between the piezoelectric effect and the mechanical response allows for the mutual influence of multiple actuators and the transformation of energy between the electrical and the mechanical fields. A new fourth-order distribution of electric potential is used to develop an electrical model that is completely compatible with the assumed higher-order strain field. The behavior of actuators subjected to large electric fields is captured using the nonlinear piezoelectric–mechanical coupling terms. The resulting model shows good correlation with available experimental data.

1. Introduction

Smart composite structures have tremendous potential in the field of aerospace structures. Piezoelectric (PZT) materials can be used as both sensors and actuators, thus both measuring and changing the strain field in a structure. Traditionally, one-way coupling, which describes the effect of the electric field on the mechanical forces in the actuators, is used for modeling the structural response of smart composites. However, two-way coupling between the electric field and the mechanical response plays an important role, in which the strains within the structure also affect the electric field within the actuators. Hagood and co-workers, see [1, 2], showed how this interaction could be utilized with passive electrical damping systems and self-sensing actuators. A general two-way coupled theory was introduced in the hybrid plate theory developed by Mitchell and Reddy [3]. Recently Chattopadhyay *et al* [4, 5] incorporated this two-way coupling effect in the development of a thermo–piezoelectrical–mechanical model for smart composites. In their work, a higher-order theory was used to describe the displacement field. These studies indicate that the effect of coupling alters the prediction of structural response as well as altering the control authority of piezoelectric actuators. This can be seen in the predicted deflection of a cantilevered plate with actuators on the upper and lower surfaces, as used in [5]. The plate was a $[0, 90]_{2s}$ graphite–epoxy laminate with a thickness of 3.048 mm and a PZT thickness of 0.762 mm. Figure 1 shows the predicted deformed shape when a 50 V load was applied to the PZTs. The uncoupled model overpredicts the deflection in this case by approximately 20%. Thus accurate modeling of smart composite structures requires the use of a coupled piezoelectric–mechanical model.

Another factor that influences the piezoelectric response is the nonlinearity in the induced strain. Although a constant piezoelectric coefficient is commonly used in the literature, the nonlinearities were clearly demonstrated in the experimental investigation performed by Crawley and Lazarus [6] At large driving voltages the piezoelectric coefficients are seen to increase, resulting in a nonlinear relation between the electric field and the induced strain. The field induced nonlinearity has been measured in piezoelectric materials by Li *et al* [7]. Research has been conducted to model the electric field dependences of piezoelectric coefficients [8]; although no differences are observed for free actuators, significant differences arise when PZTs are mounted onto host structures. The stiffness of the substructure results in much smaller strains, thus an apparent reduction in the strain–electric field nonlinearity. Results seem to indicate that this strain

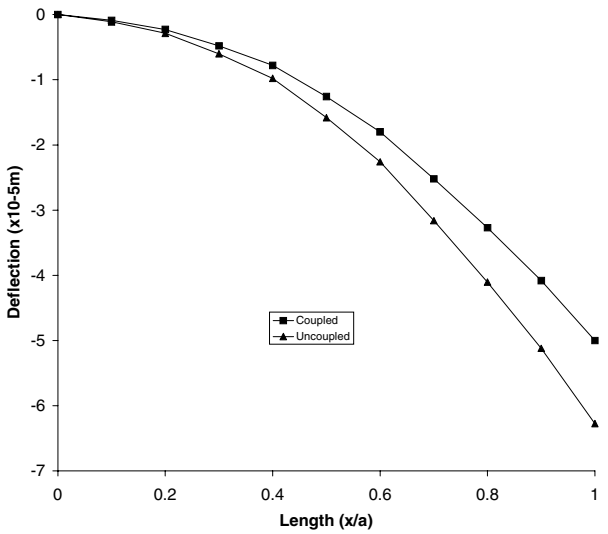

Figure 1. Predicted deformed shape of a cantilevered plate under piezoelectric loading (50 V).

dependent model of nonlinearity is more appropriate than electric field induced models [6]. Nonlinear induced strain has also been used in the modeling of box beam composite structures [9].

The objective of the current research is to integrate nonlinear piezoelectric behavior into a two-way coupled piezoelectric–mechanical model. The coupled model uses a refined higher-order laminate theory to provide accurate results for laminate constructions of moderate thickness while maintaining computational efficiency. For the sake of generality, in the present formulation the piezoelectric coefficients are assumed to be proportional to a combination of electric field and induced strain. Therefore, the model developed allows comparison between the modeling options and compatibility with the nonlinearities observed in any particular piezoelectric material. Also, a new fourth-order description of the electric potential in each PZT is developed, which is completely consistent with the higher-order displacement field.

2. Mathematical modeling

The two constitutive equations for piezoelectric–mechanical coupling are as follows:

$$\sigma_{ij} = c_{ijkl}\varepsilon_{kl} - e_{ijk}E_k \tag{1}$$

$$D_i = e_{ijk}\varepsilon_{jk} + k_{ij}E_j \tag{2}$$

where σ_{ij} and D_i are the components of the stress tensor and electric displacement vector, and ε_{ij} and E_j are the components of the strain tensor and the electric field vector. The quantities c_{ijkl}, e_{ijk} and b_{ij} are the elastic constant, the piezoelectric constant, and the dielectric permittivity, respectively. Equations (1) and (2) can be written in vector form as

$$\boldsymbol{\sigma} = \boldsymbol{Q}\boldsymbol{\sigma} - \boldsymbol{P}\boldsymbol{E} \tag{3}$$

$$\boldsymbol{D} = \boldsymbol{P}^T\varepsilon + \boldsymbol{B}\boldsymbol{E} \tag{4}$$

where $\boldsymbol{\sigma}$ and $\boldsymbol{D}$ are the stress vector and the electric displacement vector, ε and $\boldsymbol{E}$ are the strain vector and the electric field vector, and $\boldsymbol{Q}$, $\boldsymbol{P}$, and $\boldsymbol{B}$ are the stiffness, piezoelectric and dielectric permittivity matrices. The electric field vector E_i is derived from the derivatives of a scalar potential function ϕ as follows:

$$E_i = -\phi_{,i} \qquad (i = 1, 2, 3) \tag{5}$$

The governing equations are derived using Hamilton's principle as developed by Tiersten [10]:

$$\delta\Pi = 0 = \int_{t_0}^{t} \left\{ \int_V [\rho\ddot{u}_i\delta u_i - \delta H(\varepsilon_{ij}, E_i)]\,\mathrm{d}V + \int_V f_{Bi}\delta u_i\,\mathrm{d}V + \int_S f_{Ti}\delta u_i\,\mathrm{d}S + \int_V D_i\delta\phi_{,i}\,\mathrm{d}V + \int_{S_D} \bar{q}\delta\phi\,\mathrm{d}S \right\} \mathrm{d}t \tag{6}$$

$$H(\varepsilon_{ij}, E_i) = \tfrac{1}{2}c_{ijkl}\varepsilon_{ij}\varepsilon_{kl} - e_{ijk}E_i\varepsilon_{jk} - \tfrac{1}{2}k_{ij}E_iE_j \tag{7}$$

where Π is the total energy function of mechanical and electrical fields and H is the electric enthalpy. The quantity ρ is the mass density. The values f_{Bi} and f_{Ti} represent the components of the body force and traction vectors, respectively, and q_e represents the charge density. The variation of both the displacement field and the electric potential results in two independent sets of equations. It must be noted that in the two-way coupled model, the governing equations (equation (6)) are solved simultaneously, rather than sequentially as in a one-way coupled model. This ensures conservation of energy, but at the same time allows energy in the piezoelectric material to be transferred from mechanical strain energy into electric field energy and *vice versa*.

Since the objective of this research is to develop a finite element implementation of this theory, the matrix form of the governing equations will be used throughout the remainder of this paper. In matrix form, equations (6) and (7) become

$$\delta\Pi = 0 = \int_{t_0}^{t} \left\{ \int_V [\delta(\tfrac{1}{2}\rho\dot{\boldsymbol{u}}^T\dot{\boldsymbol{u}}) - \delta\varepsilon^T\boldsymbol{Q}\varepsilon + \delta\varepsilon^T\boldsymbol{P}\boldsymbol{E} + \delta\boldsymbol{E}^T\boldsymbol{P}^T\varepsilon - \delta\boldsymbol{E}^T\boldsymbol{P}\boldsymbol{E}]\,\mathrm{d}V + \int_V \delta\boldsymbol{u}^T\boldsymbol{f}_B\,\mathrm{d}V + \int_S \delta\boldsymbol{u}^T\boldsymbol{f}_S\,\mathrm{d}S + \int_S \delta\phi^T q\,\mathrm{d}S \right\} \mathrm{d}t \tag{8}$$

where $\boldsymbol{Q}$, $\boldsymbol{P}$, and $\boldsymbol{B}$ are the same as expressed in (3) and (4), $\boldsymbol{u}$ is the mechanical displacement, and ϕ is the electric potential.

To model the structural mechanical field, the refined higher-order laminate theory developed by Reddy [11, 12] is used. This theory assumes a parabolic distribution of the transverse shear strain, thus providing an accurate estimation of the transverse shear stresses for moderately thick constructions with little increase in computational effort. The theory starts with an assumed third-order displacement field as follows:

$$u_1 = u + z\psi_x + z^2\zeta_x + z^3\xi_x \tag{9a}$$

$$u_2 = v + z\psi_y + z^2\zeta_y + z^3\xi_y \tag{9b}$$

$$u_3 = w \tag{9c}$$

where u_1, u_2, and u_3 are the displacements in the x, y, and z directions, respectively. The above equations are simplified by imposing the stress free boundary conditions on the free surfaces. Since the laminate is orthotropic, this implies that

the transverse shear strains are zero. The refined displacement field now takes the following form:

$$u_1 = u + z\left(\psi_x - \frac{\partial w}{\partial x}\right) - \frac{4z^3}{3h^2}\psi_x \tag{10a}$$

$$u_2 = v + z\left(\psi_y - \frac{\partial w}{\partial y}\right) - \frac{4z^3}{3h^2}\psi_y \tag{10b}$$

$$u_3 = w \tag{10c}$$

where u, v, and w are the displacements of the midplane and ψ_x and ψ_y are the rotations of the normal at $z = 0$ about the y and $-x$ axes, respectively. The variable z represents the location with respect to the midplane of the plate and h is the total plate thickness.

The displacement vector, $\boldsymbol{u}$, can be written in terms of the midplane displacements and rotations using an operator matrix, $\boldsymbol{L_u}$, as follows:

$$\boldsymbol{u} = \begin{Bmatrix} u_1 \\ u_2 \\ u_3 \end{Bmatrix} = \begin{bmatrix} 1 & 0 & -z\frac{\partial}{\partial x} & z - \frac{4}{3h^2}z^3 & 0 \\ 0 & 1 & -z\frac{\partial}{\partial y} & 0 & z - \frac{4}{3h^2}z^3 \\ 0 & 0 & 1 & 0 & 0 \end{bmatrix} \begin{Bmatrix} u \\ v \\ w \\ \psi_x \\ \psi_y \end{Bmatrix} = \boldsymbol{L_u}\boldsymbol{u_u} \tag{11}$$

and the strain vector $\boldsymbol{\varepsilon}$ can similarly be written in terms of the displacements and an operator matrix, $\boldsymbol{L_\varepsilon}$

$$\boldsymbol{\varepsilon} = \begin{Bmatrix} \varepsilon_1 \\ \varepsilon_2 \\ \varepsilon_4 \\ \varepsilon_5 \\ \varepsilon_6 \end{Bmatrix} = \begin{Bmatrix} \frac{\partial u_1}{\partial x} \\ \frac{\partial u_2}{\partial y} \\ \frac{\partial u_2}{\partial z} + \frac{\partial u_3}{\partial y} \\ \frac{\partial u_1}{\partial z} + \frac{\partial u_3}{\partial x} \\ \frac{\partial u_1}{\partial y} + \frac{\partial u_2}{\partial x} \end{Bmatrix} = \boldsymbol{L_\varepsilon}\boldsymbol{u_u}$$

$$= \begin{bmatrix} \frac{\partial}{\partial x} & 0 & -z\frac{\partial^2}{\partial x^2} & \left(z - \frac{4}{3h^2}z^3\right)\frac{\partial}{\partial x} & 0 \\ 0 & \frac{\partial}{\partial y} & -z\frac{\partial^2}{\partial y^2} & 0 & \left(z - \frac{4}{3h^2}z^3\right)\frac{\partial}{\partial y} \\ 0 & 0 & 0 & 0 & 1 - \frac{4}{3h^2}z^2 \\ 0 & 0 & 0 & 1 - \frac{4}{h^2}z^2 & 0 \\ \frac{\partial}{\partial y} & \frac{\partial}{\partial x} & -2z\frac{\partial^2}{\partial x \partial y} & \left(z - \frac{4}{3h^2}z^3\right)\frac{\partial}{\partial y} & \left(z - \frac{4}{3h^2}z^3\right)\frac{\partial}{\partial x} \end{bmatrix} \times \begin{Bmatrix} u \\ v \\ w \\ \psi_x \\ \psi_y \end{Bmatrix}. \tag{12}$$

Using a finite element formulation

$$\boldsymbol{u_u} = \boldsymbol{N_u}(x, y)\boldsymbol{u_u^e} \tag{13}$$

where $\boldsymbol{u_u}$ is the displacement field vector, $\boldsymbol{u_u^e}$ is the nodal displacement vector, and $\boldsymbol{N_u}(x, y)$ is an interpolation matrix.

The next step is to assume a function for the electric potential of each PZT. The potential function used must be chosen carefully in order to maintain conservation of charge through the thickness of the PZT. In order to conserve charge the electric displacement must be constant through the thickness of the piezoelectric material. Equation (2), which relates the electric displacement to the strain and electric field, now imposes the necessary condition on the potential function. Since the electric displacement must be constant and the mechanical strain varies through the thickness as seen in equation (12), the electric field must be a third-order polynomial in order to cancel out the non-constant terms in the strain. Specifically, it implies that E_3, the electric field through the thickness, should be of the same polynomial order as ε_1, ε_2, and ε_6. Since the electric field is the gradient of the electric potential as seen in equation (5), the potential function, ϕ, is obtained and can be described by a fourth-order polynomial of the z coordinate as follows:

$$\phi(x, y, z) = \phi_0(x, y) + z\phi_1(x, y) + z^2\phi_2(x, y) + z^4\phi_4(x, y) \tag{14}$$

where ϕ_0, ϕ_1, ϕ_2, and ϕ_4 are functions defining the variation of the in-plane electric potential. The third-order term is omitted, because, as shown above, no strain terms exist to interact with it. Note that the z coordinate still refers to location with respect to the midplane of the laminate structure. Although this may at first seem inconvenient, it is consistent with the description of the strain field and allows for ease of integration as will be seen later. Next, it is assumed that electrodes cover the upper and lower surfaces of each PZT, thus the potentials on the upper and lower surfaces are constant, V_u and V_L respectively. By substituting this assumption into (14) the variables ϕ_0 and ϕ_1 are eliminated, and the potential function now reduces to the following form:

$$\begin{aligned}\phi(x, y, z) = {} & V_L\left(1 + \frac{z_L - z}{t}\right) + V_u\frac{z - z_L}{t} \\ & + \phi_2(x, y)[z^2 - z(2z_L + t) + (z_L^2 + tz_L)] \\ & + \phi_4(x, y)[z^4 - z(4z_L^3 + 6z_L^2 t + 4z_L t^2 + t^3) \\ & + (3z_L^4 + 6z_L^3 t + 4z_L^2 t^2 + z_L t^3)]\end{aligned} \tag{15}$$

where z_L refers to the z coordinate of the lower surface of the PZT and t is the thickness of the PZT. Physically, ϕ_0 represents the effect of bending strain on the electric field and ϕ_1 represents the effect of transverse shear strain.

Using equation (5), the electric field vector, $\boldsymbol{E}$, can be derived by differentiating the potential function, equation (15), with respect to x, y, and z. For solution purposes it is useful to separate out the free variables into a vector of unknowns; this results in the following:

$$\boldsymbol{E} = \boldsymbol{L_E}\boldsymbol{u_\varphi} = \begin{bmatrix} 0 & [z^2 - z(2z_L + t) + (z_L^2 + tz_L)]\frac{\partial}{\partial x} \\ 0 & [z^2 - z(2z_L + t) + (z_L^2 + tz_L)]\frac{\partial}{\partial y} \\ \frac{1}{t} & -2z + 2z_L + t \\ \begin{bmatrix} z^4 - z(4z_L^3 + 6z_L^2 t + 4z_L t^2 + t^3) \\ +(3z_L^4 + 6z_L^3 t + 4z_L^2 t^2 + z_L t^3) \end{bmatrix}\frac{\partial}{\partial x} \\ \begin{bmatrix} z^4 - z(4z_L^3 + 6z_L^2 t + 4z_L t^2 + t^3) \\ +(3z_L^4 + 6z_L^3 t + 4z_L^2 t^2 + z_L t^3) \end{bmatrix}\frac{\partial}{\partial y} \\ -4z^3 + 4z_L^3 + 6z_L^2 t + 4z_L t^2 + t^3 \end{bmatrix} \begin{Bmatrix} \Delta V \\ \phi_2(x, y) \\ \phi_4(x, y) \end{Bmatrix} \tag{16}$$

and

$$\Delta V = V_L - V_u \tag{17}$$

$$\phi(x, y, z) = \boldsymbol{L}_\varphi \boldsymbol{u}_\varphi \tag{18}$$

$$\boldsymbol{u}_\varphi \phi = \boldsymbol{N}_\varphi(x, y,)\boldsymbol{u}_\varphi^{\mathrm{e}} \tag{19}$$

where $\boldsymbol{u}_\varphi$ is the electric potential vector, $\boldsymbol{u}_\varphi^{\mathrm{e}}$ represents the nodal potential vector, and $\boldsymbol{N}_\varphi(x, y)$ is an interpolation vector. Using this formulation, the coefficients ϕ_2 and ϕ_4 are interpolated over each PZT using the same finite element mesh as the displacements, thus creating degrees of freedom in addition to the electrical potential between the electrodes for each PZT, ΔV. The substitution of ΔV is made to represent the difference in the voltage between the electrodes, since the absolute voltage on a single electrode is irrelevant and not required in the equations.

Using equations (1), (2), (6), (11)–(13), and (16)–(19) and integrating over the volume yields

$$\delta \Pi_u = \delta \boldsymbol{u}_u^{\mathrm{e}^T} \int_0^{t_0} (-\boldsymbol{M}\ddot{\boldsymbol{u}}_u^{\mathrm{e}} - \boldsymbol{K}_{uu}\boldsymbol{u}_u^{\mathrm{e}} - \boldsymbol{K}_{u\varphi}\boldsymbol{u}_\varphi^{\mathrm{e}} + \boldsymbol{F}_u)\,\mathrm{d}t = 0 \tag{20}$$

$$\delta \Pi_\varphi = \delta \boldsymbol{u}_\varphi^{\mathrm{e}^T} \int_0^{t_0} (-\boldsymbol{K}_{\varphi u}^{\mathrm{e}}\boldsymbol{u}_u^{\mathrm{e}} - \boldsymbol{K}_{\varphi\varphi}\boldsymbol{u}_\varphi^{\mathrm{e}} + \boldsymbol{F}_\varphi)\,\mathrm{d}t = 0 \tag{21}$$

which in turn yields the governing equations for the coupled theory, written in matrix form as follows

$$\begin{bmatrix} \boldsymbol{M} & \boldsymbol{0} \\ \boldsymbol{0} & \boldsymbol{0} \end{bmatrix} \begin{Bmatrix} \ddot{\boldsymbol{u}}_u^{\mathrm{e}} \\ \ddot{\boldsymbol{u}}_\varphi^{\mathrm{e}} \end{Bmatrix} + \begin{bmatrix} \boldsymbol{K}_{uu} & \boldsymbol{K}_{u\varphi} \\ \boldsymbol{K}_{\varphi u} & \boldsymbol{K}_{\varphi\varphi} \end{bmatrix} \begin{Bmatrix} \boldsymbol{u}_u^{\mathrm{e}} \\ \boldsymbol{u}_\varphi^{\mathrm{e}} \end{Bmatrix} = \begin{Bmatrix} \boldsymbol{F}_u \\ \boldsymbol{F}_\varphi \end{Bmatrix} \tag{22}$$

where $\boldsymbol{M}$ is the structural mass matrix. The matrix $\boldsymbol{K}_{uu}$ is the mechanical stiffness matrix, $\boldsymbol{K}_{\varphi\varphi}$ is the electrical stiffness matrix, and $\boldsymbol{K}_{u\varphi}$ and $\boldsymbol{K}_{\varphi u}$ are the stiffness matrices due to piezoelectric–mechanical coupling. The vectors $\boldsymbol{F}_u$ and $\boldsymbol{F}_\varphi$ are the force vectors due to mechanical and electrical loading. These terms are further defined in the appendix.

Since the piezoelectric coefficients are assumed to be proportional to the electrical field and/or the induced strain, these coefficients are now functions of the z coordinate as well, and are written as follows

$$P_{i3} = P_{i3}^0 + P_{i3}^\varepsilon \varepsilon_i(1, z, z^3) + P_{i3}^E E_3(1, z, z^3) \qquad i = 1, 2, 6 \tag{23}$$

$$P_{42} = P_{42}^0 + P_{42}^\varepsilon \varepsilon_4(1, z^2) + P_{42}^E E_2(1, z, z^2, z^4) \tag{24}$$

$$P_{51} = P_{51}^0 + P_{51}^\varepsilon \varepsilon_5(1, z^2) + P_{51}^E E_1(1, z, z^2, z^4). \tag{25}$$

The strain induced nonlinearity requires that an iterative process be used for the solution. An iterative solution process is chosen for static solutions based on the relatively mild nonlinearity of the strain–electric field relation. The problem is solved first for the linear case and then the resulting strain is used to calculate new piezoelectric coefficients. Although these coefficients are still functions of z, this is incorporated during the integration process through the thickness. This iterative sequence continues until convergence is achieved.

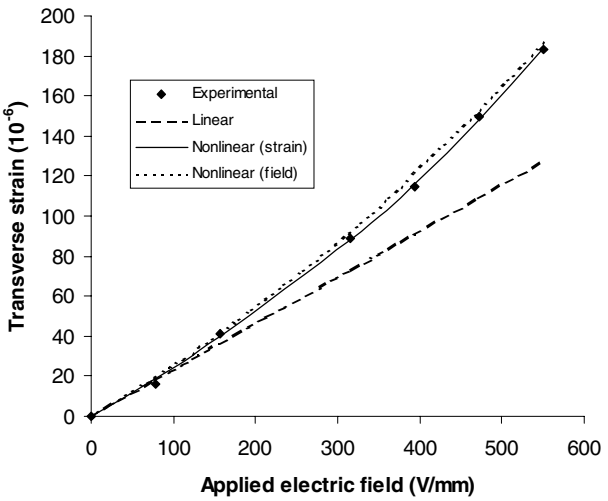

Figure 2. Transverse strain of graphite–epoxy–PZT sandwich.

3. Results

The results of this model are first verified against the experimental data of [6]. These experiments model a PZT actuator symmetrically sandwiched between two structural plates of the same thickness and material. The sandwich is then tested with free boundary conditions and no external loads. The PZT is 0.25 mm thick and has a Young's modulus of $E = 63$ GPa. The piezoelectric coefficient d_{31} for the PZT in [6] can be expressed as either

$$d_{31} = 247 \times 10^{-12}\,[\mathrm{m\ V^{-1}}] + E_3(207 \times 10^{-18}\,[\mathrm{m^2\ V^{-2}}]) \tag{26}$$

$$d_{31} = 247 \times 10^{-12}\,[\mathrm{m\ V^{-1}}] + \varepsilon_1(5.58 \times 10^{-7}\,[\mathrm{m\ V^{-1}}]). \tag{27}$$

These equations are determined based on the experimentally determined data for the electric field–strain relation in an unconstrained actuator. Since the actuator is not constrained, both of these forms seem equally valid, but the test is whether one is more appropriate when bonded to a structure and the strain is opposed by the structure. More details on determining the coefficients can be found in [6]. The conversion from the commonly used d_{31} coefficient to the elements of the matrix $\boldsymbol{P}$ is easily accomplished using (1), since d_{ij} is simply the ratio between E_i and ε_j for an unconstrained actuator.

Results are shown in figures 2 and 3 for the resulting transverse strain and longitudinal strain. The sandwich material used is graphite–epoxy lamina 0.41 mm thick. The Young's moduli are $E_L = 95.8$ GPa and $E_T = 6.7$ GPa, which causes the large difference in the resulting strains between the transverse and longitudinal directions. It can be seen that although both the strain induced nonlinearity and the electric field induced nonlinearity correlate well for the transverse strain, the field based nonlinear model overpredicts extension in the longitudinal direction. The increase in stiffness caused by the graphite fibers results in significantly lower strain values and therefore the strain dependent nonlinear model creates a smaller electrical field and thus lower induced strain. Thus, for this piezoelectric material, the strain dependent nonlinear model appears to be more appropriate as determined by [6].

Next, the developed procedure is implemented in the analysis of a unimorph actuator subjected to large actuating

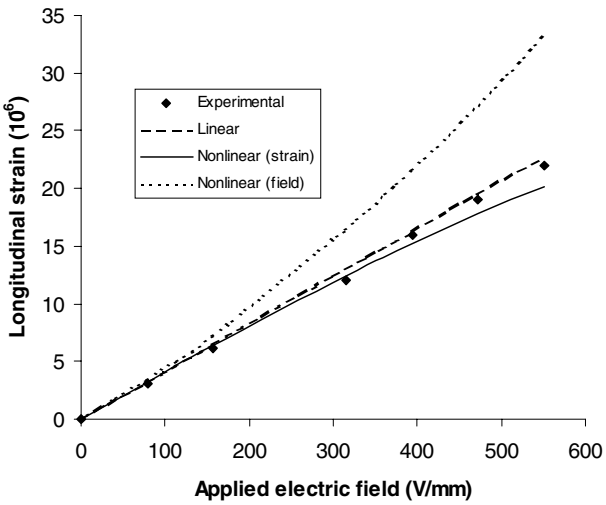

Figure 3. Longitudinal strain of graphite–epoxy–PZT sandwich.

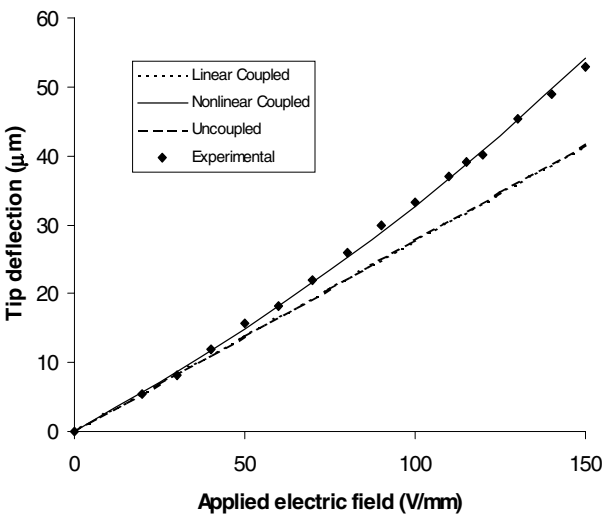

Figure 4. Tip deflection of the unimorph actuator.

voltages. This specimen was chosen due to the availability of experimental data in [13]. A soft PZT material, 0.68 mm thick, is bonded to a stainless-steel plate, 0.38 mm thick. From this a 7 mm wide by 35 mm long cantilevered unimorph actuator is constructed. The Young's moduli for the PZT and stainless steel are 63 GPa and 200 GPa, respectively, and the piezoelectric coefficient is given by

$$d_{31} = 320 \times 10^{-12}\,[\mathrm{m\ V^{-1}}] + \varepsilon_1 (1.61 \times 10^{-6}\,[\mathrm{m\ V^{-1}}]). \quad (28)$$

This equation is determined based on the experimentally determined electric field–strain relation for the unconstrained actuator used in [13]. It is also assumed that d_{36}, d_{42}, and d_{51} are all zero. The variation in tip deflection with applied electric field is presented in figure 4. The applied electric field is defined as the ratio of the differential voltage between the electrodes to the actuator thickness. This is the electrical field value that is assumed in the uncoupled theory, but it is not the actual electrical field that exists within the PZT. Figure 4 shows the results for the nonlinear coupled model against the linear coupled model and the linear uncoupled model. The nonlinear

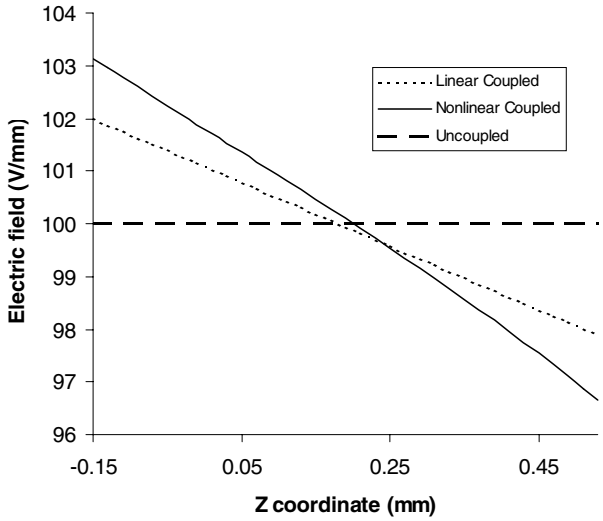

Figure 5. Electric field within the unimorph PZT.

model shows good correlation with the experimental data from [13]. It can also be seen that the uncoupled model slightly overpredicts the tip deflection compared to the linear coupled model. The reason for this is the fact that the uncoupled model does not correctly predict the energy stored in the electric field within the PZT. The coupled model allows for the transformation of electric energy into mechanical strain energy while maintaining the conservation of the total energy in the system. The variation of the electrical field across the PZT can be seen in figure 5. This figure demonstrates the impact of the coupled model on the electrical energy distribution within the piezoelectric material. The electric field in the coupled model varies through the thickness of the PZT just as the strain varies through the thickness of the structure. This variation in electric field is necessary in order to conserve the charge on the electrodes of the PZT. For the coupled model the charge on the electrodes is $\pm 3.81 \times 10^{-7}$ C, while in the uncoupled model the charge is $+3.88 \times 10^{-7}$ C and -3.73×10^{-7} C on the lower and upper electrodes, respectively. Figure 6 shows the blocking force that can be generated using this unimorph actuator. Again the nonlinear coupled model correlates well with the experimental data.

Next, the unimorph actuator is subjected to a uniform load of 150 Pa while at the same time being actuated in the opposite direction. Figure 7 shows the resulting distribution for the electric field under an applied electric field of 100 V mm^{-1}. In this case the resulting tip deflection is only 4.99 μm, thus the bending strains are much smaller compared to the unloaded case. Therefore, the electric field variation is less across the thickness of the PZT. Some of the electric field variation seen in figure 7 is caused by the presence of the transverse shear strains due to the uniform load.

Finally, the nonlinear coupled model is applied to a composite plate subject to a combination of uniform pressure loading and piezoelectric actuation. The plate used is a simply supported graphite–epoxy laminate with actuators on the top surface; it is shown in figure 8. The actuators and composite lamina have the same properties as those listed in [6]. Two ply configurations are examined, $[0, 90]_s$ and $[45, -45]_s$, with ply thicknesses of 0.50 mm and PZT thicknesses of 0.25 mm.

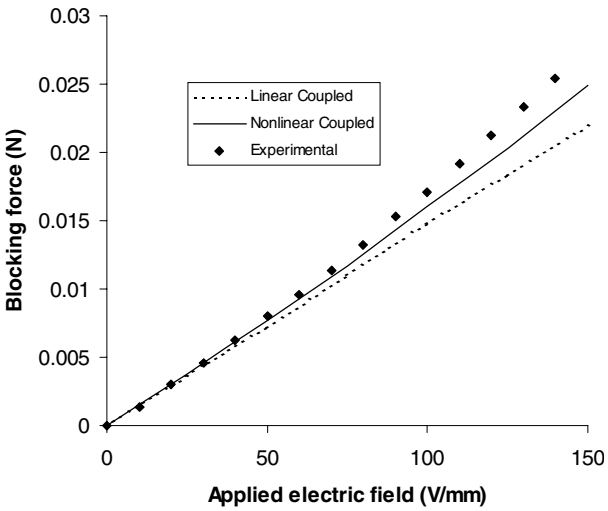

Figure 6. Blocking force for the unimorph actuator.

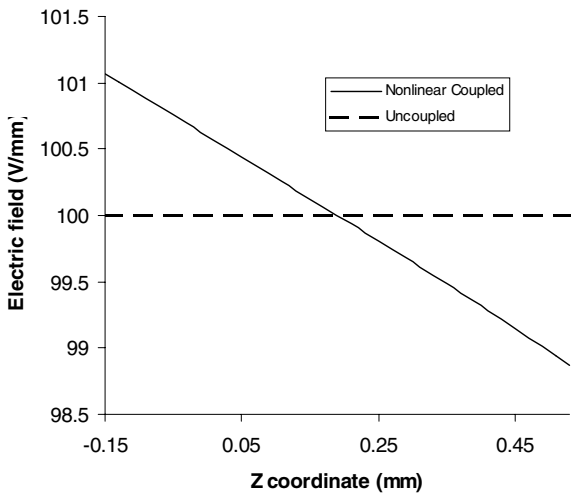

Figure 7. Electrical field within the unimorph under uniform load (150 Pa).

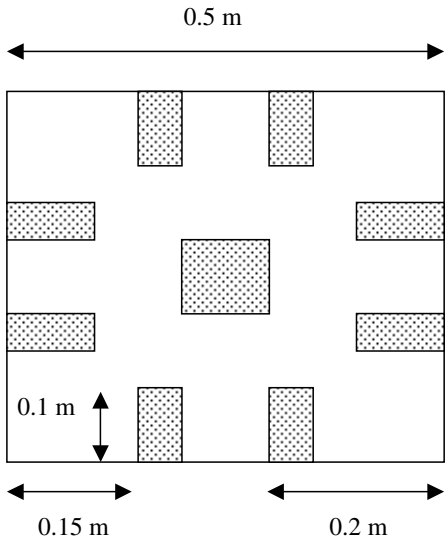

Figure 8. Simply supported composite plate with actuators.

Table 1. Plate deflection under 100 V PZT actuation..

	Ply configuration	
	$[0, 90]_s$	$[45, -45]_s$
Uncoupled	0.2059 mm	0.2712 mm
Linear coupled	0.2057 mm	0.2709 mm
Nonlinear coupled	0.2233 mm	0.2959 mm

Table 2. Plate deflection under 1000 Pa uniform load and 100 V PZT actuation.

	Ply configuration	
	$[0, 90]_s$	$[45, -45]_s$
No PZT actuation	−6.7205 mm	−7.8375 mm
Uncoupled	−6.5156 mm	−7.5663 mm
Linear coupled	−6.5147 mm	−7.5642 mm
Nonlinear coupled	−6.5729 mm	−7.6940 mm

Due to symmetry, a 10 × 10 finite element discretization of the quarter-plate is used. The results for the static actuation of the PZTs with 100 V are shown in table 1. The values listed are the out-of-plane deflection at the center of the plate. Again the uncoupled model differs from the coupled model due to the energy stored in the electric field of the PZTs. Also, the nonlinearity of the PZTs creates a significant change in the deflection of the plate. Table 2 presents the plate deflection values when a uniform load of 1000 Pa is applied to the top of the plate. The PZTs now actuate to oppose the deflection of the plate. Since the actuators are now under compressive loading the effects of the coupling and nonlinearity are reversed from previous cases, thus making this model applicable to any arbitrary loading case.

The advantage of this nonlinear coupled model is that it allows accurate modeling of composite laminates containing piezoelectric materials used in any arbitrary manner. The coupled theory simultaneously solves the mechanical equations and the electrical equations for the piezoelectric materials. Although this technique adds a few new degrees of freedom to the system, they are small compared to the total degrees of freedom required to model the original structure. This is not only due to the relatively simple formulation used, but also because, in general, a greater number of small PZTs is more effective than covering the entire surface with a single PZT. The coupled formulation presented is also advantageous in control system design. The coupled theory accurately utilizes both the voltage and the charge on the electrodes of the PZT, thus the actual electrical equations for the control system can be incorporated into the current model and solved simultaneously with the mechanical structural model. This would allow analysis of the feedback control system and determination of the power consumption of the control system. The coupled model also has the advantage that it is derived without making assumptions on how the piezoelectric material is used (that is, actuator or sensor). Thus, a designer can easily modify a control system without having to change the structural model. Thus the developed nonlinear coupled piezoelectric model offers an efficient and flexible method for analysis of smart composite laminates.

4. Concluding remarks

A completely coupled piezoelectric–mechanical theory that includes the nonlinear piezoelectric effects has been developed for composite plates with embedded or surface bonded actuators and sensors. The refined higher-order laminate theory used accurately captures the effects of transverse shear stresses in moderately thick laminates while being computationally efficient. The developed fourth-order distribution of electric potential makes the electrical field completely compatible with the assumed higher-order strain field while satisfying the electrical boundary conditions. The use of the mechanical strain-induced nonlinearity in piezoelectric coefficients resulted in an accurate prediction of strain (within 2%) in the graphite–epoxy–PZT sandwich and tip deflection of the unimorph actuators. The estimation of the blocking force exerted by the unimorph actuators is predicted with slightly less accuracy (9%). The developed model demonstrates that the higher-order variation in electric field, across the thickness of the PZT in the unimorph actuator, is necessary to maintain conservation of the charge on the PZT electrodes. Errors of over 3% were observed in the charge predicted by the linear uncoupled theory in the thin PZT layer of a unimorph actuator. Larger errors are expected in structures utilizing thicker PZTs.

Acknowledgment

This research was supported by the Air Force Office of Scientific Research, grant F49620-97-1-0419; technical monitor Daniel Segalman.

Appendix

The following are the definitions for the matrices in equation (24):

$$\boldsymbol{M} = \int_{A_e} \int_{h/2}^{h/2} \boldsymbol{N_u^T L_u^T} \rho \boldsymbol{L_u N_u} \, \mathrm{d}z \, \mathrm{d}A \tag{A1}$$

where $\boldsymbol{L_u}$ is the displacement operator matrix of equation (11)

$$\boldsymbol{K_{uu}} = \int_{A_e} \int_{h/2}^{h/2} \boldsymbol{N_u^T L_\varepsilon^T Q L_\varepsilon N_u} \, \mathrm{d}z \, \mathrm{d}A \tag{A2}$$

where $\boldsymbol{L_\varepsilon}$ is the strain operator matrix of equation (12)

$$\boldsymbol{K_{u\varphi}} = \left[\int_{A_e} \int_{zL_1}^{zu_1} \boldsymbol{N_u^T L_\varepsilon^T P_1 L_{E1} N_\varphi} \, \mathrm{d}z \, \mathrm{d}A, \right.$$
$$\left. \ldots, \int_{A_e} \int_{zL_m}^{zu_m} \boldsymbol{N_u^T L_\varepsilon^T P_m L_{Em} N_\varphi} \, \mathrm{d}z \, \mathrm{d}A \right] \tag{A3}$$

where m = number of PZTs and $\boldsymbol{L_E}$ is the electric field operator matrix of equation (18)

$$\boldsymbol{K_{\varphi u}} = -\boldsymbol{K_{u\varphi}^T} \tag{A4}$$

$$\boldsymbol{K_{\varphi\varphi}} = \begin{bmatrix} \int_{A_e} \int_{zL_1}^{zu_1} \boldsymbol{N_\varphi^T L_{E1}^T P_1 L_{E1} N_\varphi} \, \mathrm{d}z \, \mathrm{d}A & \ldots \\ \ldots & \ldots \\ 0 & \ldots \\ 0 & \\ \ldots & \\ \int_{A_e} \int_{zL_m}^{zu_m} \boldsymbol{N_\varphi^T L_{Em}^T P_m L_{Em} N_\varphi} \, \mathrm{d}z \, \mathrm{d}A & \end{bmatrix} \tag{A5}$$

$$\boldsymbol{F_u} = \int_{A_e} \int_{-h/2}^{h/2} \boldsymbol{N_u^T L_u^T f_B} \, \mathrm{d}z \, \mathrm{d}A + \int_{A_e} \boldsymbol{N_u^T L_u^T f_T} \, \mathrm{d}A \tag{A6}$$

$$\boldsymbol{F_\varphi} = \begin{bmatrix} \int_{A_e} \boldsymbol{N_\varphi^T L_\varphi^T} q_1 \, \mathrm{d}A \\ \int_{A_e} \boldsymbol{N_\varphi^T L_{\varphi m}^T} q_m \, \mathrm{d}A \end{bmatrix} \tag{A7}$$

where $\boldsymbol{L_\varphi}$ is the electric potential operator matrix of equation (18).

References

[1] Hagood N W and Von Flotow A 1991 Damping of structural vibrations with piezoelectric materials and passive electrical networks *J. Sound Vib.* **146** 243–68

[2] Anderson E H and Hagood N W 1994 Simultaneous piezoelectric sensing/actuation: analysis and application to controlled structures *J. Sound Vib.* **174** 617–39

[3] Mitchell J A and Reddy J N 1995 A refined hybrid plate theory for composite laminates with piezoelectric laminae *Int. J. Solids Struct.* **32** 2345–67

[4] Chattopadhyay A, Li J and Gu H 1998 A coupled thermo–piezoelectric–mechanical model for smart composite laminates *Proc. AIAA/ASME/ASCE/AHS/ASC 39th Structures, Structural Dynamics and Materials Conf. (Long Beach, CA, 1998)* (AIAA) pp 2902–10

[5] Chattopadhyay A, Gu H and Li J 1998 A coupled thermo-piezoelectric-mechanical theory for smart composites under thermal load *Proc. 9th Int. Conf. on Adaptive Structures and Technologies (Cambridge, MA 1998)*

[6] Crawley E F and Lazarus K B 1989 Induced strain actuation of isotropic and anisotropic plates *Proc. 30th AIAA/ASME/ASCE/AHS/ASC Structures, Structural Dynamics and Materials Conf. (Mobile, AL, 1989)* pp 2000–10

[7] Li S, Cao W and Cross L E 1991 The extrinsic nature of nonlinear behavior observed in lead zirconate titanate ferroelectric ceramic *J. Appl. Phys.* **69** 7219–24

[8] Tiersten H F 1993 Electroelastic equations for electroded thin plates subject to large driving voltages *J. Appl. Phys.* **74** 3389–93

[9] Chattopadhyay A, Gu H and Liu Q 1999 Modeling of smart composite box beams with nonlinear induced strain *Composites* B **30** 603–12

[10] Tiersten H F 1967 Hamilton's principle for linear piezoelectric media *Proc. IEEE* **55** 1523–4

[11] Reddy J N 1984 A simple higher-order theory for laminated composite plates *J. Appl. Mech.* **51** 745–52

[12] Reddy J N 1997 *Mechanics of Laminated Composite Plates: Theory and Analysis* (Boca Raton, FL: Chemical Rubber Company)

[13] Wang Q M, Zhang Q, Xu B, Liu R and Cross L E 1999 Nonlinear piezoelectric behavior of ceramic bending mode actuators under strong electric fields *J. Appl. Phys.* **86** 3352–60